PAPER • **OPEN ACCESS**

Fractal Dimension Analysis of Ternary Blends Structure: Polypropylene/Chitosan/Sisal Fiber Membranes

To cite this article: T. Mokrani *et al* 2021 *IOP Conf. Ser.: Mater. Sci. Eng.* **1107** 012008

Fractal Dimension Analysis of Ternary Blends Structure: Polypropylene/Chitosan/Sisal Fiber Membranes

T. Mokrani[1], O. Agboola[123], O.S.I. Fayomi[4], A.O. Ayeni[1], A. **Ayoola[1],**

[1]Department of Chemical Engineering, Covenant University, Ota, Nigeria

[2]Department of Civil and Chemical Engineering, University of South Africa, Johannesburg, South Africa
[3]Department of Chemical, Metallurgical and Materials Engineering, Tshwane University of Technology, Pretoria, South Africa
[4]Department of Mechanical Engineering, Covenant University, Ota, Nigeria
[5]Department of Mechanical Engineering, Tshwane University of Technology, Pretoria, South Africa
Corresponding Author: oluranti.agboola@covenantunversity.edu.ng; funmi2406@gmail.com

Abstract

Generally, the microstructures of thin and dense skin membranes have a disorderly nature. Due to their extremely complex nature, it is necessary to study the relationship between surface morphology and fractal dimension of microfiltration membrane. The fractal dimension analysis of the polymer composite was study to provide information about the primary pore size and their associations with flux in porous media. The fractal dimensions of membranes were obtained by the box-counting method. The membranes with increased amount of sisal fiber have inter-twined fibrous network with larger pores. The fractal dimension values of the membranes were also high with increasing amount of sisal fiber, with 86%PP/10% SF/ 4% C having the highest value of 1.9951.

Keywords: Fractal dimension, Ternary blend, Flux, Membranes, Polymer blend

1 Introduction

Usually, particle size is considered a geometric feature, designated to solid objects with sizes varying from nanometres to millimetres. Practically, particulate systems are mostly made of particles in the range of nanometres to millimetres; thus these systems are usually polydisperse. Measurement of particle size and its distribution are very vital in research and development. This will aid the quality control of several industrial processes [1-3]. It is a vital tool in the production of particles of precise sizes for the purpose of controlling the efficiency of processes and quality of products [4]. In order to characterize the polydispersity of particles, a recognized theory of particle size distribution is needed. Shape and contour of a tailing particle (coarse, sealed and uneven pattern) could be characterized via the utilization of the notions of perimeter and area in fractal geometry [5]. The area and perimeter of a given shape with respect to a two-dimensional space are connected together through the power law [6]. The power law exponent is allied with fractal dimension, however, it essentially doesn't give an approximation of the fractal dimension that is not biased, which is dependent on the perimeter and area (*D*-value) [7].

Fractal is a geometric term, used in characterizing objects, systems and the phenomenon, spatially [8]. In mathematics, the fractal dimension (*D*) theory equals the set's topological dimension. For sets of fractal, the theoretical fractal dimension is generally more than its topological dimension and it is characteristically a fractional number; however, it could be presume an integer value [9]. It is employed in statistical measurement that shows a relationship of the morphological structural intricacy of a material. There have been several studies on the computational methods for estimating the fractal dimension [10-13], which

includes box-counting [14]. Fractal analysis possess the capability of quantifying the non-regular and intricacy of fractures using quantifiable value that will characterize the geometrical topographies of fissures and surfaces of materials [15, 16]. The quantification of a fractal material, *M (L)*, is connected to the length scale, *L*, using the scaling law in Eq. 1:

$$M(L) \sim L^{D_s} \tag{1}$$

Eq. (1) gives the property of self-similarity; thus, the calculated value from Eq. (1) is taken to be constant in the range of length scales, *L* [17]. The method of box-counting wraps the entire object under analysis, having of tiles similar dimensionality as the encompassing space. Images are wrapped with squares of a definite size employing the least number of squares to totally wrap the image of the object, since they are two dimensional in nature [18].

The development of microfiltration membranes, where engineered polymer blends are incorporated into the membrane matrix or are dispersed on the surface the membrane, is of great importance. Several industrial set-ups have utilized micro and macro porous membranes for different applications. However, the disorganized nature of pore structures in these membranes proposes the presence of a fractal structure, made by the pores [11]. The measurable characteristics of the microstructure and the surface topography of the microfiltration membranes could offer a better understanding with regards to the relationship amid surface morphology, microstructure, particle size distribution and fractal dimension properties. The objective of this work is to investigate the relationship between surface morphology and flux with respect to fractal dimension of the microfiltration membranes. It is assumed that the distribution of particle size have fractal features. The reason for the assumption that particle size distribution has fractal features is due to the fact that it is obtained as variation from the laser diffractive particle size analyser. The variations from laser diffractive particle size analyser are due to the scattering of powder particle surfaces, which in general, have fractal property [4]. Thus, it is necessary to assume the existence the fractal nature in the powder size distribution curves. Using this concept, the powder size distribution determined from the laser particle sizer can be described in terms of the following test function [4]:

$$N(p) = kp^{a} \tag{2}$$

In Eq. (2), the cumulative frequency of undersize particles is denoted as ($N(p)$) and the respective powder particle as (p), where k is the scale parameter and a is the shape parameter. The shape parameter is connected to the fractal dimension d, as $a = d - 1$ [19]. Hence Eq. (2) can be rewritten thus:

$$N(p) = kp^{d-1} \tag{3}$$

This can be further simplified by taking the logarithms on both sides, thus:

$$In\, N(p) = Ink + (d-1) In\, p \tag{4}$$

2 Experimental

2.1 Materials and Methods

Chitosan of high purity and of medium molecular weight was acquired from Sigma Aldrich, South Africa. Polypropylene was obtained from KR Polymer, Kryasan, Johannesburg, South Africa. It is a pre-consumer waste. The sisal fiber was obtained from the CSIR, Port Elizabeth, South Africa.

2.2 Preparation of sisal fibers

Liquid nitrogen was poured in a thermal cooling box and the strands of decorticated sisal fibre were soaked in the liquid nitrogen for a day at the room temperature for the purpose of making the material very brittle for milling process. The sisal fibre from the liquid nitrogen has the same appearance as before it was soaked in the liquid nitrogen. The brittle sisal fibre was milled at CSIR, Pretoria. The fibre was milled to 200-micron powder, using pin mill machine. The sisal powder was heated at 60°C for the purpose of keeping the fibres dried.

2.3 Preparation of Blends

Ternary blends of polypropylene/chitosan/sisal at various ratios were prepared in a counter-rotating mixer (Haake Rheomixer) for distributive mixing. The composites were mixed at 190°C for 10 min with a constant rotor speed of 60 rmp. Samples were designated in percentages as shown in Tab. 1. The moulds of the blends were crushed and further grounded to powder.

Table 1. Percentage compositions of raw materials used for the preparation of the membranes

SAMPLES	POLYPROPYLENE (%)	CHITOSAN (%)	SISAL FIBER (%)	TOTAL
01	100	0	0	100
02	92	8	0	100
03	92	0	8	100
04	86	4	10	100
05	86	10	4	100

The membranes were then prepared from the powder samples by hot press in a hydraulic press. The blends were hot press at 120°C for 5 minutes at a pressure of 35 bar, they were then cooled at room temperature over a period of 15 minutes. The average thickness of the samples produced was 0.55 mm.

2.4 Scanning electron microscopy (SEM)

The scanning electron microscopy employed to envision the surfaces of the microfiltration membranes was a Joel Field Emission Electron Microscope JESM-7600F. The samples prepared were fixed on a double-sided carbon tape. Iridium (≈5 nm thick) was used to coat the surfaces of the samples in order to make them conductive. With the use of accelerating voltage of 15 kV, the samples were subjected to an electron beam for the purpose of obtaining a signal for the SEM studies.

2.5 NIH ImageJ Software

ImageJ is an unrestricted platform that uses Java image processing and program analysis. It is stimulated by NIH image for Macintosh [20]. On the ground of the presumption of the power law, the pore size distribution is solely an estimation. A suitable way to assess membrane porosity is the utilization of the geometric fractals because of the generation of the cross section of sets of the tube bundle. Box counting technique using ImageJ was used for obtaining the pore area fractal dimension. The box sizes in the table for counting the fractal (box) dimensions utilizing ImageJ are, by default: 2, 3, 4, 6, 8, 12, 16, 32 and 64. Fractal dimension (*FD*) estimated using this procedure, was found from the gradient of the double-logarithmic graph using Eq. 5:

$$\log N = FD \log \varepsilon \quad (5)$$

where N represents the number of full boxes, ε represents the length of one box and FD represents the two-dimensional fractal dimension (2D-FD). Two restrictions exist for the 2D-FD parameter using this method. The first restriction is that the 2D-FD of a very dense cake, could be equivalent to 2; in the presence of some porosity, there is reduction of 2D-FD value amid the range of 2 and 1. The second restriction has to do with the requisite to possess homogeneous surfaces [21]. The process diagram for the fractal analysis of the microfiltration membranes is shown in Fig. 1.

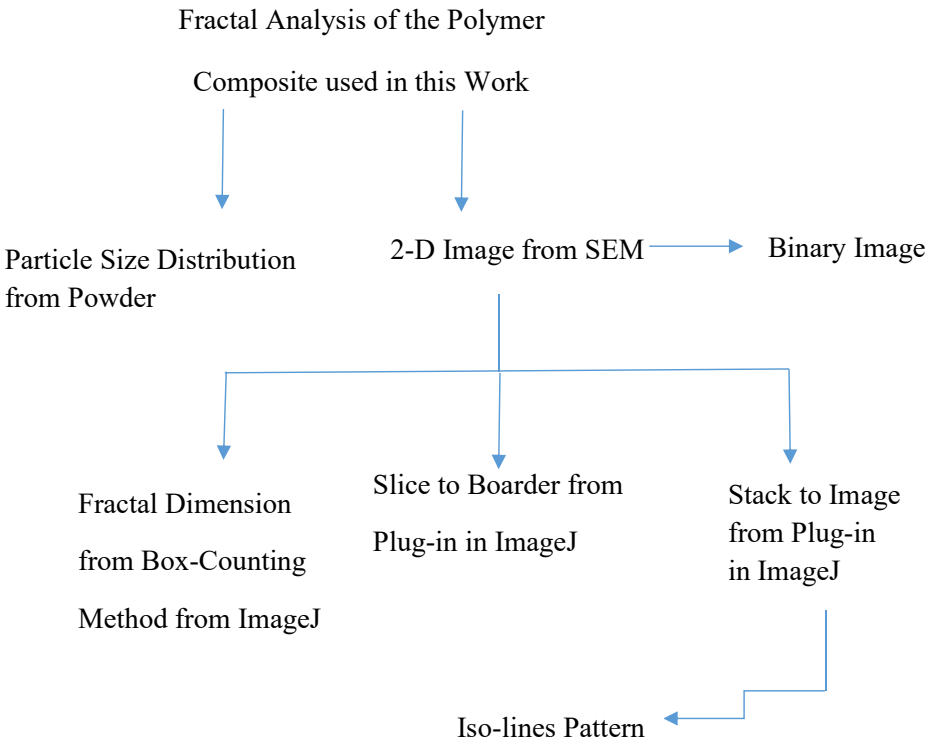

Figure 1. Process diagram for the fractal analysis of microfiltration membranes characterizations

2.6 Filtration Experiment

The filtration experiments were carried out in a 250 mL dead-end stirred batch filtration equipment, from Sterlitect Corporation, with a magnetic stirrer, schematically displayed in Fig. 2. The membrane effective filtration area is 1.26×10^{-3} m^2. Each tested membrane was fitted in the cell. The cell was operated at 2 bar, regulated with high purity nitrogen gas and stirred at 250 rpm. Initially, the membrane was rinsed with deionized water. Pure water permeability was measured using deionized water. The flux temperature was adjusted to 25ºC, by using a temperature correction factor. The membrane permeate flux, J_p ($m^3m^{-2}h^{-1}$) was determined gravimetrically using a weighing scale. The permeate flux was determined by using Eq. (6).

$$J_p = \frac{V_p}{SA \times \Delta t} \tag{6}$$

where V_p is the permeate volume (m^3) taken in the course of the filtration at sampling time, Δt (h) and SA is the effective membrane surface area.

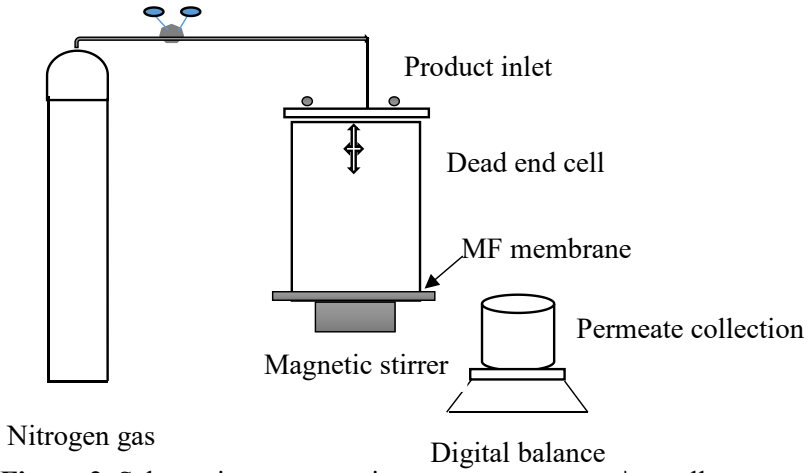

Figure 2. Schematic representation of dead end filtration cell

3 Results and discussion

3.1 Scanning electron microscopy

The morphological surface of a membrane is very important in analysing the structural property of membranes. It make available a measurement that will quantify and describe the structure of the membrane. SEM micrographs of the five polypropylene/chitosan/sisal membranes are shown in Fig. 3**.** All the membranes displayed an asymmetric structure as the surface pores could not be seen because of the dense nature of the membranes. It can be seen that nearly no pore connection was observed in the pure PP membrane (Fig. 3a) and the presence of sisal fiber and chitosan in the polymer blends are not uniformly distributed (Figs 3b-3e). Increasing amount of chitosan made the surface morphology of the membranes became denser (Figs. 3c and 3e). This was due to the fact that finer particles of chitosan were blocking the inter-particle space of the membranes; thus making the structure more condensed. Figs. 4a-4e show the binary images that would be utilised to estimate the 2D fractal dimension parameter.

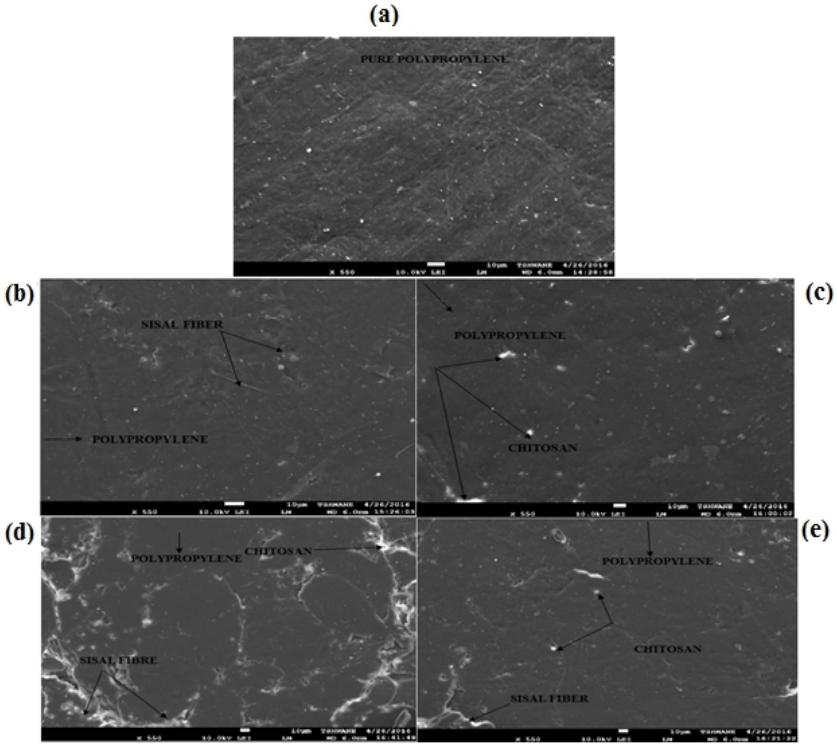

Figure 3. SEM micrographs of: Fractal dimension of: (a) 100% [PP] (b) 92% [PP] + 8% SF, (c) 92% [PP] + 8% [C], (d) 86% [PP] + 10% [SF] + 4% [C] (e) 86% [PP] + 4% [SF] + 10%[C]

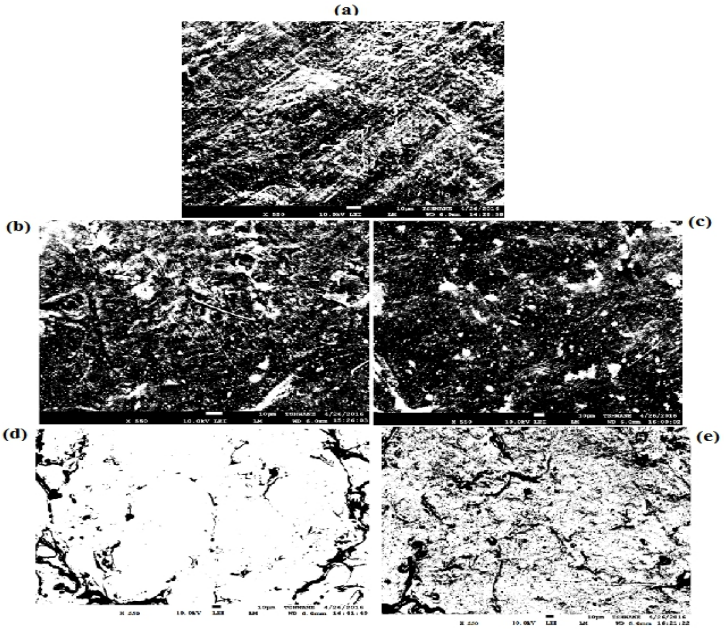

Figure 4. Binary images of SEM micrographs of: Fractal dimension of: (a) 100% [PP] (b) 92% [PP] + 8% SF, (c) 92% [PP] + 8% [C], (d) 86% [PP] + 10% [SF] + 4% [C] (e) 86% [PP] + 4% [SF] + 10%[C]

3.2 Pore area

It was difficult to qualitatively differentiate the visible surface porosity of these membranes at the fixed focus areas; thus the necessity to characterise the pore area of the images obtained from SEM. In order to understand better, the variation of porosities in the membrane composites, the pore areas of the SEM were characterized using ImageJ. Fig. 5 shows the pore area of the membranes and the geometric feature of the particles. Polypropylene membrane seems to be moderately smooth and denser with few visible pores (Fig. 5a), while polypropylene/sisal fiber membranes show inter-twined fibrous network with larger pores (Figs. 5b and 5d). The inter-twined fibrous network is more pronounced with increases in the amounts of sisal fiber (Fig. 5d). Figs. 5c and 5e show that the membranes with increased amounts of chitosan have numerous tiny pores.

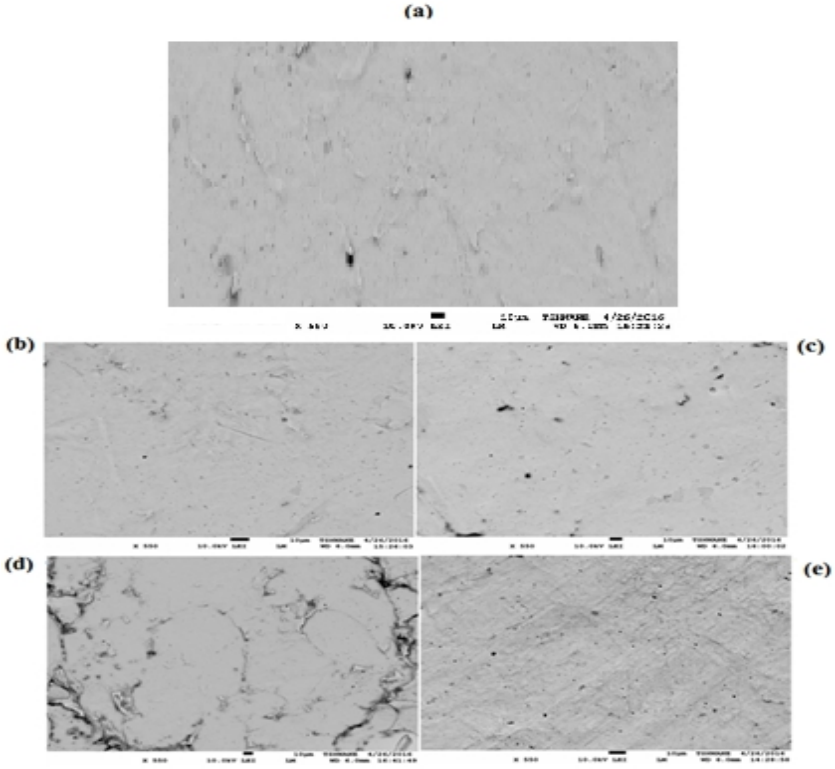

Figure 5. Pore morphology of: Fractal dimension of: (a) 100% [PP] (b) 92% [PP] + 8% SF, (c) 92% [PP] + 8% [C], (d) 86% [PP] + 10% [SF] + 4% [C] (e) 86% [PP] + 4% [SF] + 10%[C]

3.3 Fractal Analysis

Fractal dimension of the images were determined through the analysis of membranes obtained from SEM and ImageJ experiments. The box counting technique was utilized on the SEM photomicrographs (2-D images). As shown in Fig. 6, the 2D-FD parameter was obtained from SEM images by making use of the box counting procedure on the binary image. Fig. 6 depicts the relationship amid the approximated perimeter and the area of the particles in the image. The results presented show that the particles' micro-structure has typical features of fractals. By means of the least-square fitting of representation of log$N$ versus log$e$; a straight line regression via equation (5) has been obtained, as is shown in Fig 6. The D-values of the images calculated using Equation (5) are shown in Table 2. With a relative coefficient 100%, i.e. (R^2) of 1 for all the membranes. Figs. 6b and 6d show that the

membranes with increased amount of sisal fiber have higher fractal dimension values; this is in accordance with Figs. 5b and 5d that show that the membranes with increased amount of sisal fiber have inter-twined fibrous network with larger pores. The membranes without sisal fiber or little amount of sisal fiber have lower fractal dimension values; thus the higher the amount of sisal fiber in the ternary polymer blends, the more the inter-twined fibrous network and higher fractal dimension.

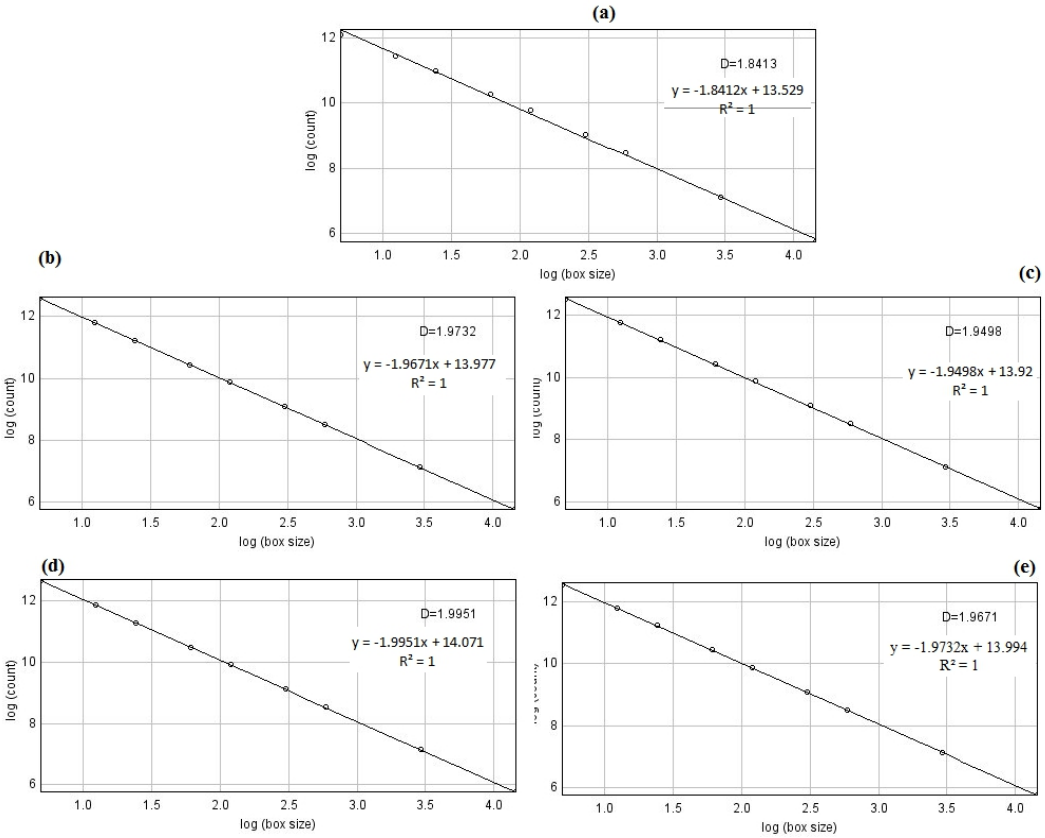

Figure 6. Fractal dimension of: (a) 100% [PP] (b) 92% [PP] + 8% SF, (c) 92% [PP] + 8% [C], (d) 86% [PP] + 10% [SF] + 4% [C] (e) 86% [PP] + 4% [SF] + 10%[C]

Table 2. The calculated D-values

Materials	***D* value**
100% PP	1.8413
92% PP + 8% sisal fiber (SF)	1.9498
92% PP + 8% chitosan (C)	1.9732
86% PP + 10% C + 4% SF	1.9671
86% PP + 10% SF + 4% C	1.9951

3.4 Membrane flux at constant pressure at 25ºC

Fig. 7 shows the membrane flux against time, at pressure of 2 bar and at temperature of 25ºC. All the membranes flux declined with time, the declination of flux with time is due to the partial pore filling by the distilled water. The reduction in the flux observed with 100% polyethylene membrane presumably occurred because the smaller pore size of the membrane observed in Fig. 3a and the lower fractal dimension observed in Fig 6a. Thus, the pore size of

this membrane most likely led to pore constriction (due to smaller pore size on the membrane surface). The presence of sisal fiber in the blend led to higher flux; the higher the amount of sisal fiber in the blends the higher the flux. This was due to inter-twined fibrous network with larger pores observed in Figs. 5b and 5d; and higher fractal dimensions observed in Figs. 6d and 6b. The presence of chitosan in the membrane also led to lower flux due the numerous tiny pores observed in Figs. 5c and 5e. The membranes without sisal fiber or little amount of sisal fiber have lower fractal dimension values and thus flux.

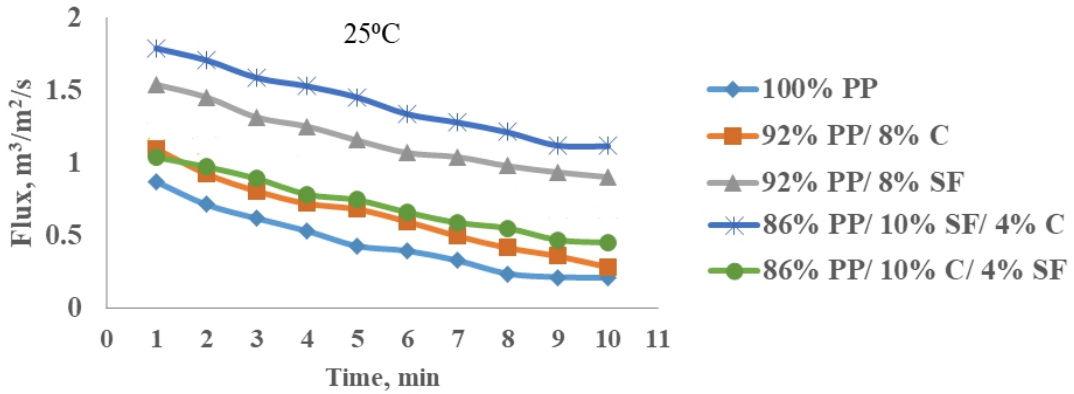

Figure 7. Flux of the composite membranes as a function of time.

Conclusion

A concise characterization of the multiscale topography of rough surfaces of membranes is very crucial for the understanding of the surface properties of thin and dense membranes; thus the multiscale nature of surface roughness of membranes warrants a scale-independent statistical characterization. The study characterized the membranes with SEM and used the SEM images to determine the fractal dimensions of the membranes. The results show that membranes with increasing amount of sisal fiber gave increase in pore sizes, fractal dimensions and higher flux.

Acknowledgement

The authors wish to acknowledge the financial support offered by Covenant University in actualization of this research work for publication.

References

[1] Sadiku-Agboola, O., Kolesnikov, A., & Sadiku, E.R. (2012). Simulation and control of nanoparticle size distribution in a high temperature reactor. Polish Journal of Chemical Technology, 14(1), 5-13.
[2] Sadiku, O., & Kolesnikov, A. (2010). Control of nanoparticle growth in high temperature reactor: Application of reduced population balance model. Journal of Computational and Theoretical Nanoscience, 7, 571–576.
[3] Sadiku, O., & Kolesnikov, A. (2011). Control of nanoparticle growth in high temperature reactor: Application of reduced population balance model II. Journal of Computational and Theoretical Nanoscience, 8, 8-16.

[4] Ramakrishan, K.N. (2000). Fractal nature of particle size distribution. Journal of Materials Science Letters, 19, 1077-1080.
[5] Sun, X., Wu, Z., & Huang, Y. (2003). Theory and Application of Fractal; University of Science and Technology Press: Beijing, China, pp. 39-41.
[6] Zhang, Q., Yin, G., Fan, X., Wei, Z., Wang, W., & Nie, W. (2015). Loading capacity and deformation characteristics of tailings based on a fractal geometrical analysis of the microstructure. Minerals, 5, 86-103.
[7] Chen, Q. (1995). The perimeter-area fractal model and its application to geology. Mathematical Geology, 27, 69-82.
[8] Bao, L., Ma, J., Long, W., He, P., Zhang, T., & Nguyen, A.V. (2014). Fractal analysis in particle dissolution: a review. Reviews in Chemical Engineering, 30(3), 261–287.
[9] Tálu, S., Stach, S., Sueiras, V., & Ziebarth, N.M. (2014). Fractal Analysis of AFM images of the bowman's membrane of the human cornea. Annals of Biomedical Engineering, 43(4), 906-916.
[10] Bo-Ming, Y. (2005). Fractal character for tortuous stream tubes in porous media. Chinese Physics Letters, 22 (1), 158-160.
[11] Zhang, L-H. (2008). A fractal model for gas permeation through porous membranes. International Journal of Heat and Mass Transfer, 51, 5288-5295.
[12] Othman, M.R., & Martunus, H.Z. (2010). Simulated fractal permeability for porous membranes. Applied Mathematical Modelling 34, 2452-2464
[13] Xu, P., Qiu, S., Yu, B., & Jiang, Z. (2013). Prediction of relative permeability in unsaturated porous media with a fractal approach. International Journal of Heat and Mass Transfer, 64, 829-837.
[14] Ristanovi, D., Stefanovi, B.D., & Puŝkaŝ, N. (2014). Fractal analysis of dendrite morphology using modified box counting method. Neuroscience Research, 84, 64-67.
[15] Gmachowski, L. (2003). Transport properties of fractal aggregates calculated by permeability. Colloids Surface A, 215:173-179
[16] Gmachowski, L. (2003). Mass- radius relation for fractal aggregates of polydisperse particles. Colloids Surface A, 224, .45-52
[17] Mandelbrot, B.B. (1977). Fractal-form: chance and dimension, Vol 1. Freeman, San Francisco
[18] Agboola, O., Mokrani, T., & Sadiku, R. (2016). Porous and fractal analysis on the permeability of nanofiltration membranes for the removal of metal ions. Journal of Materials Science, 51, 2499-2511.
[19] Mandelbrot, B.B. (1982). The fractal geometry of nature, W. H. Freeman, p. 25, New York
[20] Agboola, O., Maree, J., Mbaya, R., Zvinowanda, C.M., Molelekwa, G.F., Jullok, N., Van der Bruggen, B., Volodine, A., & Van Haesendonck, C. (2014). Deposition of toxic metal particles on rough nanofiltration membranes. Korean Journal of Chemical Engineering, 31(8), 1413-1424.
[21] Pontie, M., Thekkedath, A., Kecili, K., Dach, H., De Nardi, F. & Castaing, J.B. (2012). Clay filter-aid in ultrafiltration (UF) of humic acid solution. Desalination, 292, 73-86.